Geochemistry, Geophysics, Geosystems

RESEARCH ARTICLE
10.1029/2020GC009220

Large Silicic Eruptions, Episodic Recharge, and the Transcrustal Magmatic System

Boda Liu[1] and **Cin-Ty Lee**[1]

[1]Department of Earth, Environmental and Planetary Sciences, William Marsh Rice University, Houston, TX, USA

Key Points:
- New thermal model suggests that the temperature of the magma reservoir is controlled by the replenishment rate and the heat loss
- The growth of silicic reservoir requires decaying replenishment with a peak rate coincident with the previous eruption
- Episodic pulse of mafic magma may cause the rapid expulsion of melt from the mush, triggering the eruption

Correspondence to:
B. Liu,
boda_liu@hotmail.com

Citation:
Liu, B., & Lee, C.-T. (2020). Large silicic eruptions, episodic recharge, and the transcrustal magmatic system. *Geochemistry, Geophysics, Geosystems*, *21*, e2020GC009220. https://doi.org/10.1029/2020GC009220

Received 2 JUN 2020
Accepted 17 AUG 2020
Accepted article online 24 AUG 2020

Abstract Large silicic eruptions result from rapid evacuation of large, upper crustal reservoirs of silicic magmas. These silicic magmas are thought to be replenished by melt extracted from underlying crystal-rich source mushes, but the timescales and mechanisms of such melt extraction are unclear. Geochemical observations suggest that the replenishing melt is often more primitive than the eruptives and must thus cool and crystallize to generate the highly silicic magmas that eventually lead to large eruptions. Motivated by these observations, we use thermal models to explore the replenishment conditions capable of building an eruptible silicic reservoir to generate a large eruption. Results show that the minimum melt replenishment rate required for a silicic reservoir to start growing increases with the effective thermal diffusivity of the overlying crust and decreases with the depth of the reservoir. For an eruptible reservoir at 6 km depth to grow, the initial replenishment rate needs to be greater than 2×10^{-9} m/s. High replenishment rates are required to provide enough advected heat to counterbalance rapid heat loss and consequent freezing that would prevent the eruptible reservoir from growing. However, these high initial replenishment rates must then subside over time for the eruptible reservoir to cool, crystallize, and evolve to highly silicic melts. Thermal histories of some natural systems suggest assembly of large eruptible reservoirs in <20 kyr. The rapid replenishment followed by its decay suggests that replenishment was triggered by a pronounced but ephemeral increase in the porosity and permeability of the underlying crystal-rich source mush, allowing for rapid melt expulsion. We speculate that this perturbation may be driven by the sudden incursion of deep-seated, hotter magmas into the base of the crystal-rich source mush.

Plain Language Summary Episodic intrusion of mafic magma into crystal-rich magmatic mushes induces ephemeral fast melt expulsion and triggers large silicic eruption.

1. Introduction

Large, silicic volcanic eruptions have the potential of erupting hundreds of cubic kilometers of ash in one event, causing catastrophic damage to the environment (Bachmann et al., 2002; Christiansen, 2001; Cook et al., 2016; Hildreth & Wilson, 2007; Wilson et al., 2006). It is widely thought that the magma reservoir beneath a supervolcano is supplied by melts extracted or expelled from an underlying crystal-rich mush (Bachmann & Bergantz, 2004; Hildreth, 1981; Hildreth & Fierstein, 2000). Geochronology data suggest that magmas can reside in a crystal-rich mush state for tens of thousands of years or longer (Cooper & Kent, 2014; Crowley et al., 2007; Reid, 2013). These long-lived crystal-rich mushes are ultimately the source of many silicic eruptions. Occasionally, residual liquids within the mush are expelled, allowing for the growth of an eruptible magma reservoir (Druitt et al., 2012). To grow a large eruptible silicic reservoir (ESR), melt expulsion rates from the mush must be fast; otherwise, the shallow magma reservoir would solidify against the cold overlying crust (Annen, 2009; Fialko & Simons, 2001; Gelman et al., 2013). After the eruptible reservoir is assembled, any number of perturbations, such as a sudden increase in magma replenishment rate from below, may induce failure of the wall rock and trigger eruptions (Gregg et al., 2012; Jellinek & DePaolo, 2003).

To better understand how long-lived magmatic mushes relate to the episodicity of large volcanic eruptions, we need to understand the process by which the eruptible reservoir is replenished and grows. Compaction, hindered settling, gas filter pressing, and rejuvenation by mafic magmas or fluids have all been suggested as possible extraction and replenishment mechanisms (Anderson et al., 1984; Bachmann & Bergantz, 2004, 2006; Burgisser & Bergantz, 2011; Lee et al., 2015; McKenzie, 1984; Shaw, 1965). Advances in petrological and geochemical tools have allowed reconstruction of the thermal history of magmatic systems in which

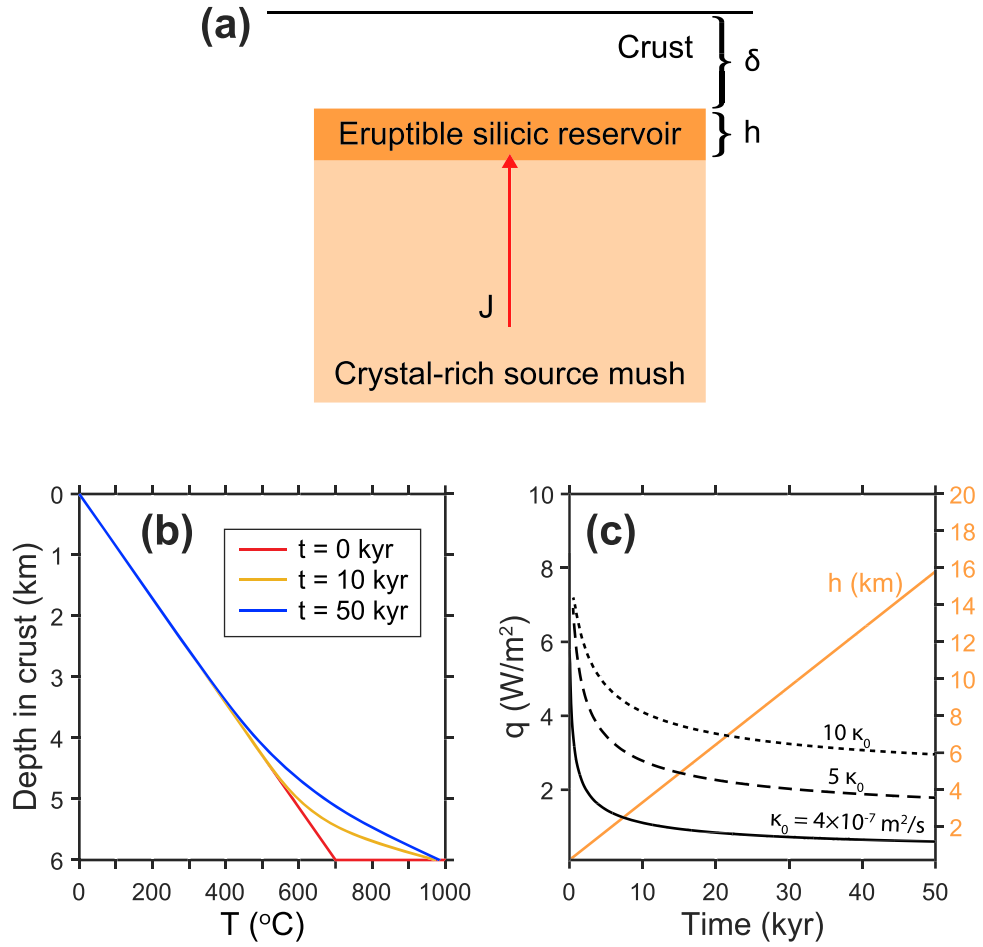

Figure 1. Model for the assembly of the eruptible silicic reservoir (ESR) with magma input extracted from the underlying crystal-rich source mush (CRSM). The ESR lies at a depth δ(6 km) in the crust and rests on top of the thicker and deeper CRSM (a). Thermal evolution of the ESR and crustal lid are modeled for the case in which the ESR is replenished by constant influx ($J = 1 \times 10^{-8}$ m/s or 0.32 m/yr) of melt from the CRSM to the ESR. Evolution of the geotherm in the crustal lid in response to the initiation and growth of the ESR is shown in (b). The effective thermal diffusivity of the crust in this case is $\kappa_0 = 4 \times 10^{-7}$ m^2/s, representing the crustal rock (Lesher & Spera, 2015). Heat flux at the interface between the crust and the ESR as a function of time shown in (c). Results with larger effective thermal diffusivity of the crust are shown by dashed and dotted lines. Heat flux into the crustal lid decays with time as the bottom of the crustal lid is heated up. The growth of the ESR is superimposed in (c).

short thermal spikes caused by magma recharge can be detected (Barboni et al., 2016). Here, we develop an open-system crystallization model to simulate the thermal and chemical evolution of the ESR. We use the thermal histories of natural systems to constrain the nature of magma recharge in the context of the transcrustal magmatic system.

2. A Hypothetical Transcrustal Magmatic System

We envision a two-layer system. Our approach is undoubtedly oversimplified, but the goal is to develop general intuition rather than make exact predictions for specific magmatic systems. We envision the upper layer representing the potentially ESR of thickness h and depth δ beneath the Earth's surface. The ESR rests above the crystal-rich source mush (CRSM) (Figure 1a). For our calculations here, we take the depth of typical ESRs to be ~6 km as estimated from storage pressures of various ESRs (2.0 ± 0.5 kbar, Huber et al., 2019).

We assume that the ESR is periodically evacuated or erupted (Spera & Crisp, 1981), and in between eruptions, the ESR grows and evolves compositionally. Our model is initiated immediately after an eruption

Table 1
Thermal Modeling Parameters

Symbol	Name	Value
c	Specific heat	1.6×10^3 J/kg/K
ρ	Density	2.3×10^3 kg/m^3
L	Latent heat	2.5×10^5 J/kg
T_{liq}	Liquidus of the melt extracted from CRSM	1000°C
T_{sol}	Solidus	700°C
κ_0	Thermal diffusivity of the crustal rock	4×10^{-7} m^2/s

Note. T_{liq} and T_{sol} are from Lee et al. (2015). Other values are from Lesher and Spera (2015).

event evacuates most of the ESR (Barker et al., 2015), and thus $h = 0$ initially. Melt expelled from the CRSM results in a magmatic replenishment flux J into the ESR, allowing it to regrow. The rate at which the ESR thickens, dh/dt, is equivalent to J, if there is no lateral growth as is commonly assumed in similar studies (Annen, 2009; Huber et al., 2009). Geochemical observations suggest that silicic magmas in ESRs derive from the crystallization of intermediate magmas, such as dacites and andesites (Bacon & Druitt, 1988; Michael, 1984; Wark, 1991). Below, we use both analytical and numerical results to shed light on the timescale and dynamics of the shallow CRSM-ESR system.

3. Modeling ESR With Heat Loss, Crystallization, and Replenishment

3.1. Heat Balance of a Hypothetical ESR

The thermal evolution of the ESR is controlled by heat loss to the Earth's surface (q), advection of heat associated with magmatic replenishment J, and the latent heat of crystallization L:

$$c\rho h\frac{dT}{dt} = -q + c\rho \cdot J(T_{in} - T) + L\rho \cdot J_x, \tag{1}$$

where T is the temperature of the ESR; c and ρ are the specific heat and density of the silicic magma (density difference between the melt and crystals are small and thus ignored); J_x is the rate of crystallization; and T_{in} is the temperature of the replenishing magma (J) derived from the expulsion of interstitial melts in the CRSM. We assume that T_{in} is the liquidus temperature of the replenishing magma (T_{liq}), which must equal the temperature of the CRSM at the time the melt is expelled (1000°C, the liquidus for the interstitial melt in CRSM; Lee et al., 2015). The rate of crystallization J_x is given by

$$J_x = \frac{d(hX)}{dt} = X \cdot J + h\frac{dX}{dT}\frac{dT}{dt}, \tag{2}$$

where X is the crystal fraction, which depends on temperature and thus on time (Huber et al., 2009; Lee et al., 2015).

To track crystallization rates, the relationship between T and X for a given compositional system is needed. For ESR systems, a hydrous dacite composition may be representative of replenishing melts (Lee et al., 2015), although for the general behavior of our models, the exact bulk composition is not critical. For hydrous compositions, T-X is not linear. Instead, much of the crystallization occurs near the solidus (Lee et al., 2015). To capture such eutectic-like behavior, we parameterize a function with two linear trends, that is, X increases slowly from 0 at $T_{liq} = 1000$°C to 80% at $T_e = 710$°C then increases quickly to 100% at $T_{sol} = 700$°C (Figure 2). The exact

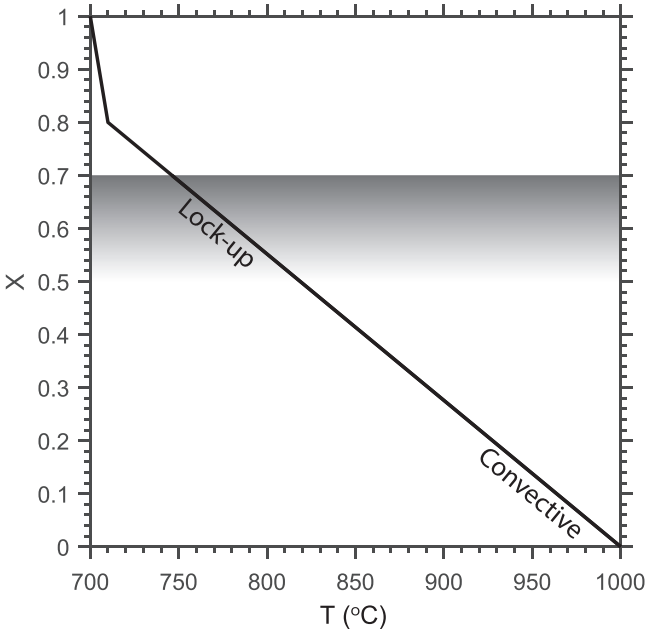

Figure 2. The X-T relationship for the melt extracted from CRSM into ESR. Due to the effect of water, the last ~20% crystallization is compressed to near solidus temperature (Lee et al., 2015). ESR gradually locks up as the crystallinity increases to 50–70% (Dufek & Bachmann, 2010).

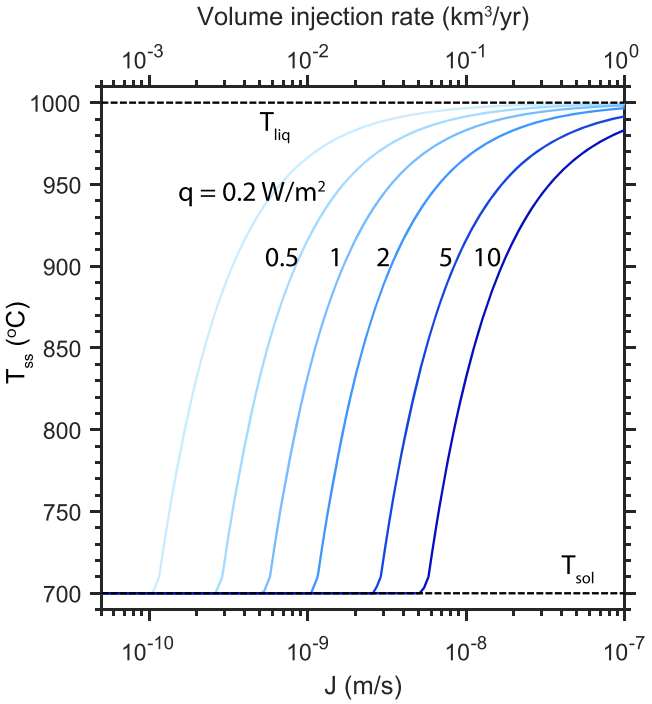

Figure 3. Steady state temperature of an ESR as a function of J and q (Equation 3). The depth of the ESR δ is 6 km. Thermal modeling parameters are summarized in Table 1. A horizontal sectional area of 314 km^2 (10 km radius circle) is used to convert the replenishment rate to volume injection rate. For reference, the heat flow under a caldera ranges from 0.2 to 2 W/m^2 (Lachenbruch et al., 1976; Morgan et al., 1977). The lower bound of the heat flow observation is consistent with a linear geotherm ($q \cong c\rho\kappa\frac{\Delta T}{\delta}$) through 6 km thick crystal lid with $\kappa_0 = 4 \times 10^{-7}$ m^2/s.

parameterization of the T-X function only has a secondary effect on the results of the model (discussed in the next section).

A fundamental assumption in the model (Equation 1) is that the ESR, including all crystals and residual melt, is thermally homogeneous. This assumption is valid so long as the crystallinity does not exceed the "lock-up" threshold, $X \sim$ 50–70% (Dufek & Bachmann, 2010) below which the ESR vigorously convects and retains crystals within the magma (Marsh, 1981; Saar et al., 2001; Turcotte & Schubert, 2002). As the crystallinity of the ESR reaches the "lock-up" threshold, convection slows down enough that reentrainment of settling crystals ceases, allowing crystal-melt separation and making possible the eruption of rhyolites. Simulations with the injection of melt suggest that convection could occur beyond the "lock-up" threshold (Bergantz et al., 2015). We do not run the thermal model for an ESR below 746°C as below this temperature, the system exceeds 70% crystallization and would be effectively locked.

The rate of heat loss q from the ESR is limited by the insulating effect of the overlying crustal lid (Bejan & Anderson, 1983; Davaille & Jaupart, 1993). We assume that such heat loss occurs by conduction with the possibility of amplification by hydrothermal circulation. We solve the thermal diffusion equation but adopt an effective thermal diffusivity κ to approximate the enhanced "conductivity" of heat when hydrothermal circulation operates (Cao et al., 2019; Combarnous & Bories, 1975). The effective thermal diffusivity has a lower bound equivalent to the thermal diffusivity of solid crustal rock $\kappa_0 = 4 \times 10^{-7}$ m^2/s (Lesher & Spera, 2015) and could increase by one order of magnitude in the presence of hydrothermal circulations (Phipps Morgan & Chen, 1993). The initial thermal state in the crustal lid is approximated with a linear geotherm, with surface temperature fixed at 0°C and the basal lid temperature corresponding to the solidus of the extracted melt as the previous ESR has already heated up the base of the crustal lid (Figure 1b). The basal lid temperature then evolves as the temperature of the ESR changes in response to the replenishment (Equation 1). The initial heat loss q is high due to the temperature contrast between the replenishing magma and the basal lid (Figure 1). Only after the bottom of the crustal lid is heated up does the heat loss decay. Partial melting and crystallization are allowed in the crustal layer, but such melts are assumed to remain with the crust. The assimilation of crustal melt adds a heat loss term ($L\rho \cdot J_a$ where J_a is the rate of assimilation) to the thermal equation and does not change the general behavior of the system for geologically reasonable magnitudes of crustal assimilation (discussed in the next section).

3.2. Steady State Temperature of the ESR

Before solving the above equations explicitly, intuition on how the system behaves can be gained by considering the steady state solutions for a given replenishment rate J into the ESR and surface heat flux q, the former a measure of how much heat is advected into the reservoir and the latter a measure of the efficiency of heat loss to the surface. The steady state temperature T_{ss} of the ESR is given by

$$T_{ss} = T_{liq} - \frac{q}{J}\frac{1}{\rho c(1+r)}, \tag{3}$$

where $r = \frac{L}{c}\cdot\left|\frac{dX}{dT}\right|$ is the ratio of latent to sensible heat in the temperature range between 710°C and 1000°C. Because r is ~0.5, the effect of latent heat is much smaller than the ratio of heat loss to advected heat gain, q/J. Thus, the temperature of the ESR increases as q/J decreases, that is, when J is large or q is low (Figure 3). Temperature decreases when J decreases or if heat flow through the crustal lid is more efficient as in the case of hydrothermal circulation. It is important to note that after reaching the steady state

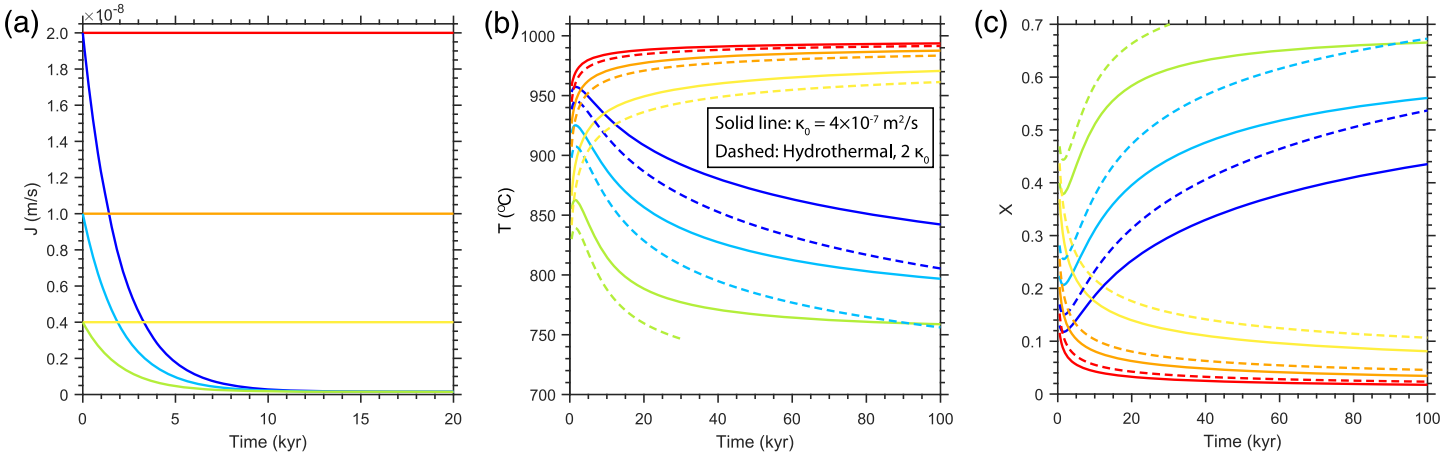

Figure 4. Time-dependent replenishment models for the ESR. (a) Different replenishment histories $J(t)$ explored, including constant (horizontal lines) and decaying scenarios. A crustal lid thickness of $\delta = 6$ km is assumed for all simulations. J_{final} for the three decaying series is 1.5×10^{-10} m/s (0.005 km/kyr). The timescale adopted for decaying J's, t_0 is 2 kyr. (b) Thermal evolution of the ESR color coded to correspond to the array of $J(t)$ scenarios explored in (a). Scenarios represented by solid lines assume there is no hydrothermal system in the crustal lid and a low effective thermal diffusivity of the crust ($\kappa_0 = 4 \times 10^{-7}$ m^2/s). Dashed lines are for enhanced thermal diffusivity ($\kappa = 2\kappa_0$) due to hydrothermal activity in the crust. (c) Evolution of crystal fraction X calculated from the temperatures in (b) for the different $J(t)$ scenarios in (a). Simulations are terminated once the ESR locks up at $X = 0.7$.

temperature T_{ss}, the volume of the ESR still increases at the rate of J. The volume of melt in ESR also continues increasing at a rate of $(1 - X_{ss})\, J_{final}$, where X_{ss} is the steady state crystallinity determined by T_{ss}.

The surface heat flux can be approximated by conduction across the crustal lid, $q \cong c\rho\kappa\frac{\Delta T}{\delta}$, where ΔT is the temperature difference between Earth's surface and the base of the crustal lid (equivalent to the temperature of the ESR). If Equation 3 is combined with the simple approximation for heat loss $q \cong c\rho\kappa\frac{\Delta T}{\delta}$ through the crustal lid, the minimum melt replenishment rate J_{min} required to maintain the ESR above a temperature T scales as

$$J_{\min} \cong \frac{\kappa}{\delta}\frac{T - T_{surface}}{T_{liq} - T}\frac{1}{1 + r}. \tag{4}$$

To maintain a specific temperature, the minimum replenishment rate must increase if the efficiency of heat loss through the crustal lid is high, as would be the case if effective thermal diffusivity is high or if lid thickness is thin. For a temperature of 850°C, the minimum replenishment rate is 2.0×10^{-9} m/s for a strong hydrothermal system with q of 2 W/m^2 (Figure 3). Allowing for assimilation of crustal melt (e.g., 20% for Yellowstone, Troch et al., 2018) only requires a 10% increase in the minimum replenishment rate. The exact choice of the X-T relationship is of secondary importance because $\left|\frac{dX}{dT}\right|$ is not expected to vary significantly below a crystallinity of 70% (in any case, a 50% increase of $\left|\frac{dX}{dT}\right|$ only results in 17% reduction of J_{min}).

Based on the foregoing analysis, the initial replenishment rate must be fast for the ESR to start growing and not freeze from the outset. For the general case described here, that is, an ESR lying at 6 km depth, no hydrothermal circulation (and hence low effective thermal diffusivity for the crust $\kappa_0 = 4 \times 10^{-7}$ m^2/s), and a bulk composition similar to a hydrous dacite, the initial replenishment rate must be greater than 2×10^{-9} m/s (0.06 m/yr) to prevent freezing. Higher rates would be required if cooling is enhanced by hydrothermal circulation. If these rates can be sustained indefinitely, a 1 km thick ESR could be generated within ~15 kyr. This ESR, however, would be characterized by warm temperatures ($T > 950$°C) and relatively primitive melt compositions. Because many of the large silicic eruptions are rhyolitic and record lower temperatures (<800°C) (Bachmann et al., 2002; Hildreth & Wilson, 2007; Wilson et al., 2006), we know that replenishment rates must ultimately decline after the initial replenishment.

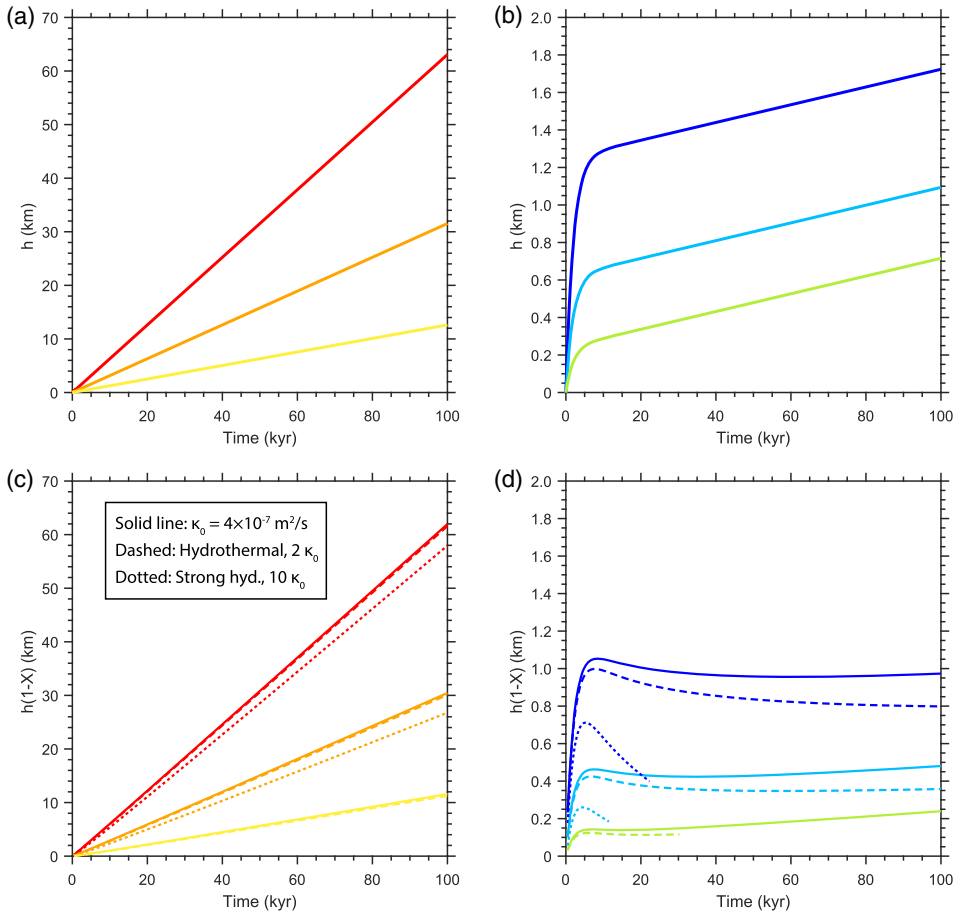

Figure 5. Evolution of the ESR thickness (a, b) and the total volume of melt in the ESR (c, d), calculated as the product of the melt fraction $(1 - X)$ and the thickness of the ESR. The six different replenishment scenarios are the same as those in Figure 4a. The three constant replenishment scenarios are in (a) and (c), while the three decaying scenarios are in (b) and (d). Results with different thermal diffusivity of the crust are represented by solid ($\kappa_0 = 4 \times 10^{-7}$ m^2/s), dashed ($\kappa = 2\kappa_0$), and dotted lines ($\kappa = 10\kappa_0$) in (c) and (d). Notice that the ESR freezes immediately in the two cases with the slowest starting replenishment rate (yellow and green) and strong hydrothermal system.

4. Decaying Replenishment to the ESR

To better constrain how the ESR responds to replenishment, we explicitly solve the above time-dependent equations (Equation 1 and heat conduction in the crust) while incorporating a declining J. We generalize J's decline as an exponential function of time:

$$J(t) = \left(J_{start} - J_{final}\right) \cdot \exp(-t/t_0) + J_{final}, \tag{5}$$

where J_{start} is the initial replenishment rate, t_0 is a characteristic timescale for decay, and J_{final} is the asymptotic replenishment rate at long times.

We compare cases with constant J and cases with decaying J ($t_0 = 2$ kyr and $J_{final} = 1.5 \times 10^{-10}$ m/s). In cases with constant J (Figure 4), the temperature of the ESR gradually increases and reaches a high steady state temperature (>950°C). The increase of ESR temperature is due to decaying q and increasing J/q. With decaying J, the ESR gradually cools down, develops high crystallinity ($T < 850$°C and $X > 0.4$, Figure 4), and would consequently result in residual melts with high silica. The timescale for the initial replenishment rate to decay, t_0, is shorter than the timescale of cooling because the evolution of temperature lags the change in the instantaneous replenishment rate. All thermal evolution paths eventually decay to the same steady state temperature T_{ss} if J_{final} and κ are held constant, but the time to reach T_{ss} increases with J_{start}.

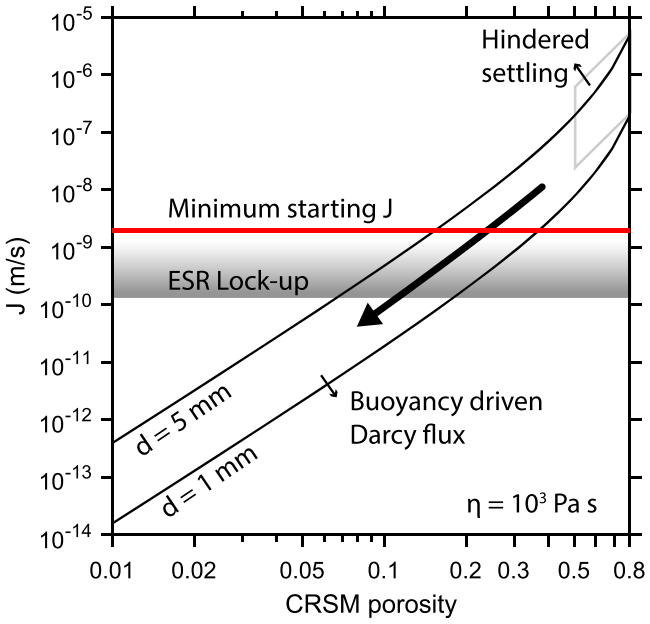

Figure 6. The prediction of the rate of melt replenishment as buoyance driven Darcy flux (Carman, 1997) or hindered settling (Richardson & Zaki, 1954). The viscosity of the dacitic melt extracted from CRSM is calculated using the model of Giordano and Dingwell (2003) at 1000°C. The grain size d ranges from 1 to 5 mm (Bachmann & Bergantz, 2004). The density contrast between the melt and the solid is 280 kg/m^3 (Lesher & Spera, 2015). The arrow indicates the slowdown of J as melt is extracted from the CRSM. As J decays, ESR would gradually cool, crystallize, and eventually lock up.

To place these results into context, our calculations show that the thickness of the ESR replenished by a decaying J at 6 km depth reaches 0.25–1.2 km within 5 kyr with only ~0.5 km growth in the next 100 kyr (equivalent to $J_{final} = 1.5 \times 10^{-10}$ m/s or 5 m/kyr). The timescale of the early growth stage is proportional to t_0, and the corresponding early stage thickness is proportional to $J_{start} \cdot t_0$. Assuming a cylindrical magmatic system of radius ~10 km, an ESR volume of 200–500 km^3 is attained after 100 kyr, consistent with building the silicic reservoirs thought to lead to supereruptions within the ~1 Myr repose times between major eruptive events (Christiansen, 2001; Cook et al., 2016; Hildreth & Wilson, 2007; Wilson, 1993); these reservoir volumes have been inferred to be of 10^2–10^3 km^3 (Bachmann & Bergantz, 2004).

Finally, we note that because of the shallow depth of typical ESRs, the effect of crustal hydrothermal systems on cooling may be important. For example, enhanced hydrothermal convection, simulated by a tenfold increase of the effective thermal diffusivity of the crustal lid, could explain the remarkably high heat flows of 0.2–2 W/m^2 in and around many volcanically active regions (Lachenbruch et al., 1976; Morgan et al., 1977). If the effective thermal diffusivity of the crust is moderately high (1×10^{-6} m^2/s) or high (4×10^{-6} m^2/s), even higher replenishments than calculated above are required (4×10^{-9} m/s (0.13 m/yr) or 6×10^{-9} m/s (0.19 m/yr), respectively). The ESR would lock up after 10 kyr in the presence of large effective thermal diffusivity (4×10^{-6} m^2/s) and slow J_{final} (1.5×10^{-10} m/s or 0.005 m/yr). However, the ESR can maintain convection if there is no hydrothermal activity and replenishment continues (Figures 4 and 5).

5. Discussion and Implications

5.1. Episodic Recharge and Melt Extraction From CRSM

In summary, the above analysis shows that the growth of the ESR requires a major perturbation or influx of melt into the ESR, which then gradually declines back to base levels. If this replenishing influx of melt was derived from the underlying CRSM, the question arises as to how these silicic and hence viscous melts were extracted so fast. A widely held view is that interstitial melts are expelled from the CRSM via compaction of the solid matrix of the mush (Bachmann & Bergantz, 2004; McKenzie, 1984). Indeed, compaction-driven melt expulsion naturally slows down as the melt fraction of the CRSM is reduced, thereby decreasing permeability (Carman, 1997; McKenzie, 1984). We calculate the buoyancy-driven Darcy flux using the viscosity of the dacitic melt (1×10^3 Pa·s, Giordano & Dingwell, 2003) and a range of grain size (<5 mm, Bachmann & Bergantz, 2004) at various porosities (Figure 6). At high porosity ($\phi > 50\%$), hindered settling becomes the applicable mechanism for melt expulsion as there is no longer a mechanically coherent crystal framework (Holness, 2018). The fast J_{start} required to initiate the growth of the ESR can be realized by hindered settling (Richardson & Zaki, 1954) or buoyancy-driven Darcy flux at $\phi > 15\%$ (Figure 6). The foregoing suggests that the porosity of the CRSM at the onset of melt extraction from the CRSM to the ESR must have been at least temporarily high. As melt is extracted from the CRSM, porosity should gradually decrease, in turn, decreasing permeability and causing a further decline in the melt extraction rate, leading to a decline in the replenishment rate of the ESR.

A number of studies have suggested that eruptions can be triggered by deep-seated pulses of mafic magma (Bachmann & Bergantz, 2006; Edmonds et al., 2010; Tait et al., 1989; Wark et al., 2007). If correct, these hypothetical deep-seated pulses could provide a reasonable mechanism for driving the expulsion of melt from the CRSM, in turn, triggering the eruption of the ESR. Although the absolute magnitude of the replenishment rate required to trigger eruptions would depend on a number of parameters including the size and

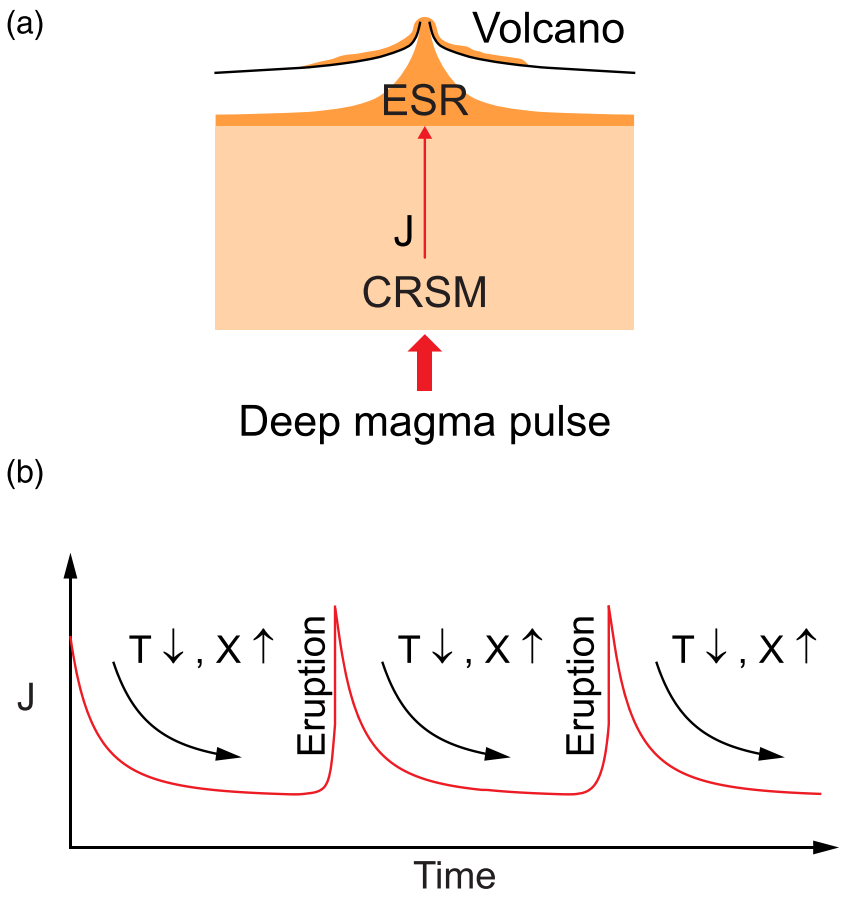

Figure 7. Conceptual cartoon showing the relationship between large silicic eruptions, episodic recharge, and deep magma pulses. (a) The rising of a deep magma rejuvenates the CRSM and causes fast melt expulsion, which results in a rapid replenishment and triggers the eruption of the existing silicic reservoir. After the eruption, continued but declined melt expulsion from the CRSM due to porosity reduction, rebuilds a new ESR. As the ESR cools by heat loss through the overlying crust, the residual melt becomes more silicic. The ESR stays above the solidus if a slow replenishment rate is sustained. During this time, if another deep magma pulse arrives at the CRSM before the ESR fully crystallizes and locks up, another eruption can be triggered and the cycle reset. (b) In each cycle, the volume of eruptible melt in the ESR and its silica content increases while undergoing down-temperature crystallization.

geometry of the ESR, the viscosity and yield strength of the wall rock, etc. (Gregg et al., 2012), the ESR is most likely to erupt when the replenishment is at its maximum. A deep-seated pulse of mafic magma into the CRSM could rejuvenate the crystal-rich mush, generating an interstitial melt representing a mixture of these recharging magmas and remelted CRSM (Bachmann & Bergantz, 2006; Burgisser & Bergantz, 2011). The interstitial melt in the CRSM can be extracted rapidly when the melt faction is high. However, this high melt fraction state cannot be sustained as the pulse of mafic magma decays and the interstitial melt is extracted. As melt expulsion rates decline, the overlying ESR begins to cool and crystallize. We propose that the arrival of a deep-seated magma pulse at the base of the CRSM could trigger eruption of the ESR (Figure 7). The eruption is then followed by slow rebuilding of a new ESR with a decaying replenishment rate. If evacuation of the ESR is ultimately caused by deep-seated magma recharge into the CRSM, the implication is that the episodicity of large silicic eruptions may be controlled by the tempo of deep magmatic fluxes from the mantle or lower crust. Monitoring of deep level processes may thus be important for predicting large volcanic eruptions.

5.2. Trace Element Evolution

Finally, the results of our modeling may have implications for the evolution of trace components in the ESR. We consider the simultaneous recharge and fractional crystallization model of Lee et al. (2014) to track the concentration of three generalized trace elements with bulk partition coefficients D of 0, 0.5, and 2 in the

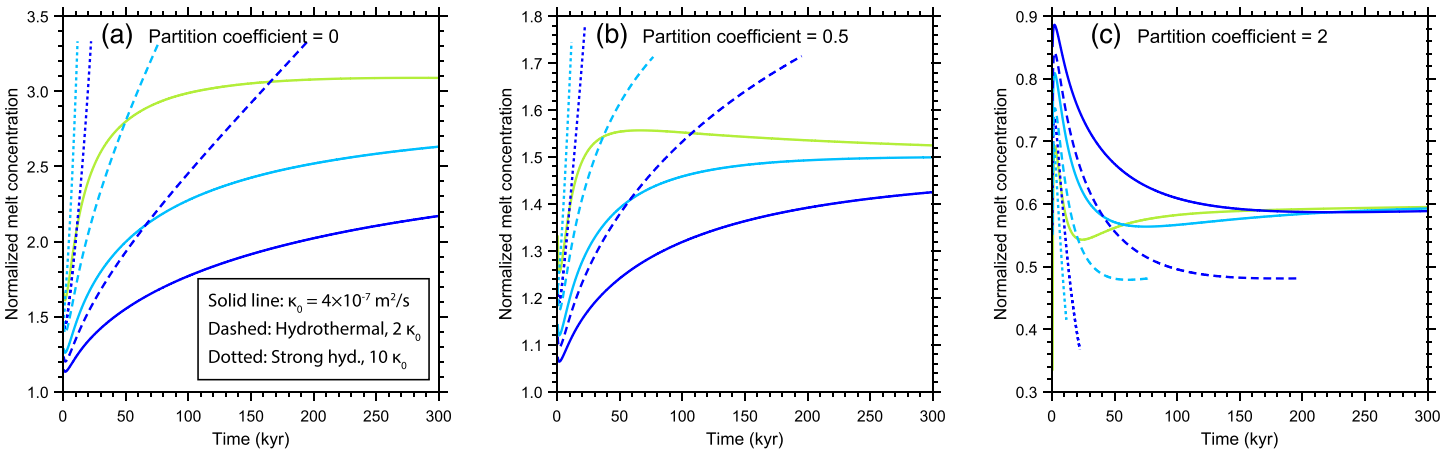

Figure 8. The concentration of generalized trace elements in the residual melt of ESR due to the effects of simultaneous magma replenishment and crystallization. We consider a perfectly incompatible (a), moderately incompatible (b), and compatible element (c), with solid/melt partition bulk coefficients of 0, 0.5, and 2, respectively. The concentration is normalized to that of the replenishing magma. As in previous figures, dashed and solid lines represent different effective thermal diffusivities of the crust. Colors are the same as Figure 4a.

residual melt (Figure 8), with $D < 1$ representing an element incompatible in the crystallizing phases and $D > 1$ compatible in crystallizing phases. In all calculations, instantaneous equilibrium crystallization was assumed but crystallized products were not allowed to equilibrate with any subsequent melts. The rise in the concentration of the incompatible trace elements and the fall of compatible trace elements in the residual melt with time reflects the increase in net crystallization in the growing ESR, even with replenishment. Smaller J_{start} or larger κ would result in faster enrichment of incompatible trace elements (Figure 8). Concentrations of incompatible trace elements can be enriched to up to 3.3 times that of the melt extracted from the CRSM by the time the ESR locks up. Of particular interest is the effect of replenishment on water, a component which can be treated as highly incompatible prior to saturation in

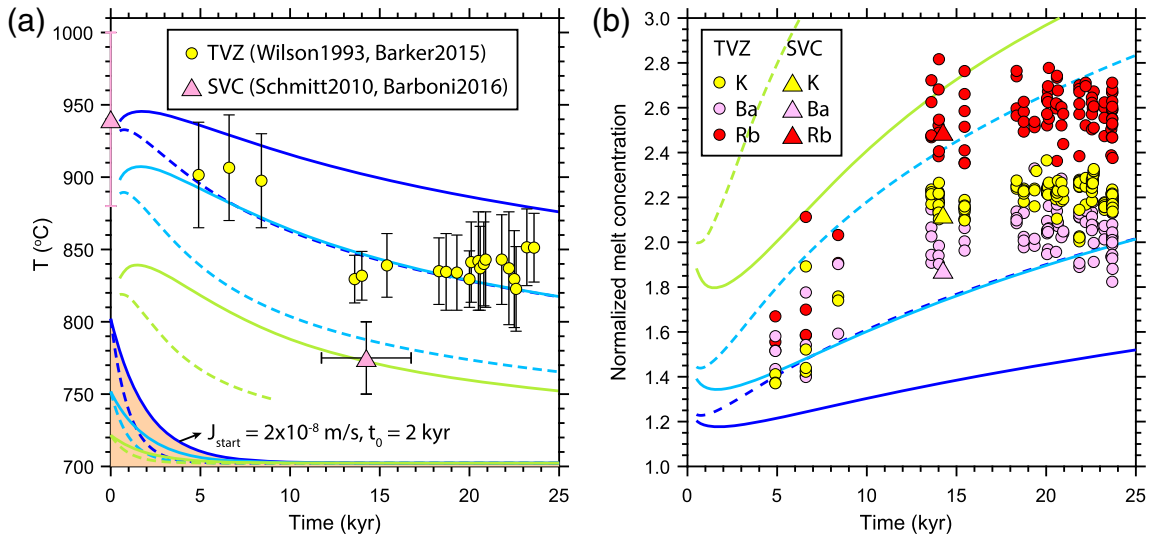

Figure 9. Applications to thermal and chemical evolution of two natural systems at the Taupo Volcanic Zone (TVZ), New Zealand (Barker et al., 2015; Wilson, 1993), and the Soufrière Volcanic Center (SVC) in the Caribbean (Barboni et al., 2016; Schmitt et al., 2010). (a) We compare the geothermometry time series recorded by samples with six simulations parameterized to represent a variety of replenishment histories (plotted on the bottom, $J_{start} = 4 \times 10^{-9}$, 1×10^{-8}, or 2×10^{-8} m/s; $t_0 = 1$ or 2 kyr; $J_{final} = 1.5 \times 10^{-10}$ m/s). The effective thermal diffusivity is 6.4×10^{-7} m^2/s for all runs. The enrichment of incompatible trace element K, Ba, Rb in TVZ and SVC compared to simulations of a perfectly incompatible element (b). The concentration of the erupted magma is normalized to the included enclave that represents the parental intermediate magma (TVZ: Sutton et al., 2000; Barker et al., 2015; SVC: Schmitt et al., 2010; Barboni et al., 2016).

a free fluid phase. For the range of initial water contents of replenishing melts (e.g., 2–3 wt.%, Sisson & Layne, 1993), our simulations show that the melt of ESR could eventually saturate in water (~6 wt.% at 2 kbar, Burnham & Jahns, 1962) after J has decayed and the ESR has cooled. Saturation itself could play a role in triggering an eruption (Huppert & Woods, 2002). More work is needed to explore these effects, but what is clear is that the nature of replenishment is important for the compositional evolution of any magmatic system.

5.3. Application to Natural Systems

To evaluate whether our model is at all applicable, we attempt here to apply our model to natural systems. Samples from the Taupo Volcanic Zone (TVZ), New Zealand, and the Soufrière Volcanic Center (SVC) in the Caribbean provide unique opportunities to constrain how a silicic magma reservoir grows because their thermal and compositional evolutions have been documented by well-resolved magmatic time series (Barboni et al., 2016; Barker et al., 2015; Schmitt et al., 2010; Sutton et al., 2000; Wilson, 1993).

5.3.1. Post-Oruanui Reassembly of ESR at TVZ

The TVZ was marked by a major rhyolitic eruption (the Oruanui eruption) 25.4 kyr ago, representing large-scale evacuation of an ESR (Allan et al., 2017; Wilson, 1993, 2001; Wilson et al., 2006). The Oruanui event was followed by small volume eruptions: 5–8 kyr later by dacitic eruptions and 14 kyr later by a return to rhyolitic eruptions (Wilson, 1993). These small volume eruptions following the Oruanui event provide a window into what remained of the magmatic system after the Oruanui eruption event and suggest a gradual reassembly of the ESR. A 50–70°C cooling, as constrained by FeTi-oxide and plagioclase-melt thermometry (Figure 9a, Barker et al., 2015), accompanied the transition from the 5–8 kyr dacites to the 14 kyr rhyolites. The first-order compositional evolution of the post-Oruanui magmatic series indicates a parental magma with similar composition as dacite clasts hosted in the Oruanui rhyolites (Barker et al., 2015; Sutton et al., 2000). In particular, small volumes of similar parental magmas also accompany the post-Oruanui rhyolitic eruptions, indicating the existence of a parental dacitic magma during the reassembly of the ESR (Barker et al., 2015; Sutton et al., 2000; Wilson, 1993).

We compare the TVZ series with six simulations parameterized to represent a variety of replenishment histories ($J_{start} = 4 \times 10^{-9}$ m/s to 2×10^{-8} m/s, $t_0 = 1$ to 2 kyr, $J_{final} = 1.5 \times 10^{-10}$ m/s). We use an effective diffusivity of the crust of 6.4×10^{-7} m^2/s for all runs. The application of our model to the thermal history of the TVZ reservoir in the first 25 kyr of rebuilding a rhyolitic ESR confirms the importance of a decaying replenishment rate of a more primitive magma, such as a dacite. There is a trade-off between the starting replenishment rate J_{start} and the timescale for the starting replenishment to decay t_0, as two replenishment histories with $J_{start} = 2 \times 10^{-8}$ m/s, $t_0 = 1$ kyr and $J_{start} = 1 \times 10^{-8}$, $t_0 = 2$ kyr produce similar thermal histories, all consistent with the data within uncertainties. The results of the thermal modeling also predict well the enrichment of incompatible elements in the post-Oruanui series (Figure 9b). Compared to the dacitic parental magma, the concentration of incompatible trace elements in post-Oruanui magmas can be enriched by 2–2.8 times (Barker et al., 2015; Sutton et al., 2000). For a perfectly incompatible element, the observed level of enrichment can be achieved by 50% to 64% crystallization after 15 kyr of synchronous growth and cooling (Figure 9b). More realistic parameterization of T-X relationship and partition coefficients would improve the match with the observed geochemical trend. In summary, the results of thermal and chemical modeling suggest a pulse of replenishment followed by its decay within 15 kyr.

5.3.2. Pre-Belfond Thermal Pulse at SVC

The observation of down-temperature crystallization is also seen in the thermal histories of the SVC (Barboni et al., 2016; Schmitt et al., 2010). One of the most recent activities, the 13.6 ka Belfond eruption, contains zircon-bearing enclaves which record pulses in crystallization temperatures extending to 14.2 kyr before the eruption (Barboni et al., 2016). The oldest zircon ages of >200 ka suggest that the magmatic system is long-lived, probably in the form of a crystal-rich mush for most of the time. The latest replenishment may dissolve older zircons and produce the observed zircon population biased to ages younger than ~30 ka. The combined geochronology and geothermometry constraints suggest that the long-lived crystal-rich mush was mobilized by a pulse of replenishment at ~28 ka. The zircon saturation temperature of 880°C provides a lower bound for the maximum temperature caused by the replenishment event (Barboni et al., 2016). The eruptible reservoir for the Belfond eruption was then assembled within 14.2 kyr after the initial replenishment. Normalized to the composition of the enclave, which we take to represent the composition of the

replenishing magma, the incompatible elements in Belfond lava becomes enriched by 2–2.5 times, consistent with the down-temperature crystallization predicted by the model. Therefore, a replenishment pulse followed by decay may have also played an important role in the assembly of the ESR that was responsible for the Belfond eruption at SVC.

5.4. Implications for the Transcrustal Magmatic System

Applying current models to the samples from TVZ and SVC suggests that ESRs can be assembled within 20 kyr once the long-lived CRSM is perturbed triggering a new pulse of melt extraction from the CRSM and consequent replenishment of the overlying ESR. Other processes like crustal assimilation and nonlinear *X-T* behavior are secondary and, most importantly, do not negate the necessity of a replenishment pulse to grow an ESR. More tests on magma samples with improved precision in geochronology are needed. If the rapid assembly of the ESR is general for silicic systems, the arrival of deep-seated more primitive magmas at the base of CRSM could be directly or indirectly the cause of large silicic eruptions by triggering melt expulsion from the CRSM, which then triggers eruption of the overlying ESR and reinitiating the buildup of another ESR. Obviously, not all magmatic pulses originating from below lead to silicic eruption because there are many other mechanical conditions that influence eruption triggering (Gregg et al., 2012). Whether deep magmatic pulses drive large supereruptions, which have a repose time of ~1 Myr (Christiansen, 2001; Cook et al., 2016), is unclear but worth exploring further.

Data Availability Statement

The code to reproduce the result is available online (at https://data.mendeley.com/datasets/mkbj6mjc46/draft?a=da757eba-3cc1-42f3-aff2-b368179f64a1).

Acknowledgments

We thank Wiess Postdoctoral Fellowship at Rice University and NSF EAR-1753599 for support. Discussions with H. Gonnermann, P. Phelps, and J. Jordan are appreciated. S. de Silva, C. B. Till, and M. Townsend are thanked for very helpful reviews.

References

Allan, A. S. R., Barker, S. J., Millet, M.-A., Morgan, D. J., Rooyakkers, S. M., Schipper, C. I., & Wilson, C. J. N. (2017). A cascade of magmatic events during the assembly and eruption of a super-sized magma body. *Contributions to Mineralogy and Petrology*, *172*(7), 49. https://doi.org/10.1007/s00410-017-1367-8

Anderson, A. T., Swihart, G. H., Artioli, G., & Geiger, C. A. (1984). Segregation vesicles, gas filter-pressing, and igneous differentiation. *The Journal of Geology*, *92*(1), 55–72. https://doi.org/10.1086/628834

Annen, C. (2009). From plutons to magma chambers: Thermal constraints on the accumulation of eruptible silicic magma in the upper crust. *Earth and Planetary Science Letters*, *284*(3-4), 409–416. https://doi.org/10.1016/j.epsl.2009.05.006

Bachmann, O., & Bergantz, G. W. (2004). On the origin of crystal-poor rhyolites: Extracted from batholithic crystal mushes. *Journal of Petrology*, *45*(8), 1565–1582. https://doi.org/10.1093/petrology/egh019

Bachmann, O., & Bergantz, G. W. (2006). Gas percolation in upper-crustal silicic crystal mushes as a mechanism for upward heat advection and rejuvenation of near-solidus magma bodies. *Journal of Volcanology and Geothermal Research*, *149*(1-2), 85–102. https://doi.org/10.1016/j.jvolgeores.2005.06.002

Bachmann, O., Dungan, M. A., & Lipman, P. W. (2002). The Fish Canyon magma body, San Juan volcanic field, Colorado: Rejuvenation and eruption of an upper-crustal batholith. *Journal of Petrology*, *43*(8), 1469–1503. https://doi.org/10.1093/petrology/43.8.1469

Bacon, C. R., & Druitt, T. H. (1988). Compositional evolution of the zoned calcalkaline magma chamber of Mount Mazama, Crater Lake, Oregon. *Contributions to Mineralogy and Petrology*, *98*(2), 224–256. https://doi.org/10.1007/BF00402114

Barboni, M., Boehnke, P., Schmitt, A. K., Harrison, T. M., Shane, P., Bouvier, A.-S., & Baumgartner, L. (2016). Warm storage for arc magmas. *Proceedings of the National Academy of Sciences*, *113*(49), 13,959–13,964. https://doi.org/10.1073/pnas.1616129113

Barker, S. J., Wilson, C. J. N., Allan, A. S. R., & Schipper, C. I. (2015). Fine-scale temporal recovery, reconstruction and evolution of a post-supereruption magmatic system. *Contributions to Mineralogy and Petrology*, *170*(1), 5. https://doi.org/10.1007/s00410-015-1155-2

Bejan, A., & Anderson, R. (1983). Natural convection at the interface between a vertical porous layer and an open space. *Journal of Heat Transfer*, *105*(1), 124–129. https://doi.org/10.1115/1.3245530

Bergantz, G. W., Schleicher, J. M., & Burgisser, A. (2015). Open-system dynamics and mixing in magma mushes. *Nature Geoscience*, *8*(10), 793–796. https://doi.org/10.1038/ngeo2534

Burgisser, A., & Bergantz, G. W. (2011). A rapid mechanism to remobilize and homogenize highly crystalline magma bodies. *Nature*, *471*(7337), 212–215. https://doi.org/10.1038/nature09799

Burnham, C. W., & Jahns, R. H. (1962). A method for determining the solubility of water in silicate melts. *American Journal of Science*, *260*(10), 721–745. https://doi.org/10.2475/ajs.260.10.721

Cao, W., Lee, C.-T. A., Yang, J., & Zuza, A. V. (2019). Hydrothermal circulation cools continental crust under exhumation. *Earth and Planetary Science Letters*, *515*, 248–259. https://doi.org/10.1016/j.epsl.2019.03.029

Carman, P. C. (1997). Fluid flow through granular beds. *Chemical Engineering Research and Design*, *75*, S32–S48. https://doi.org/10.1016/S0263-8762(97)80003-2

Christiansen, R. L. (2001). *The Quaternary and Pliocene Yellowstone Plateau volcanic field of Wyoming, Idaho, and Montana* (Vol. 729). Menlo Park, CA: U.S. Department of the Interior, U.S. Geological Survey.

Combarnous, M. A., & Bories, S. A. (1975). Hydrothermal convection in saturated porous media. In V. T. Chow (Ed.), *Advances in hydroscience* (Vol. 10, pp. 231–307). Frisco, CO: Elsevier.

Cook, G. W., Wolff, J. A., & Self, S. (2016). Estimating the eruptive volume of a large pyroclastic body: The Otowi member of the Bandelier Tuff, Valles caldera, New Mexico. *Bulletin of Volcanology*, *78*(2), 10. https://doi.org/10.1007/s00445-016-1000-0

Cooper, K. M., & Kent, A. J. R. (2014). Rapid remobilization of magmatic crystals kept in cold storage. *Nature*, *506*(7489), 480–483. https://doi.org/10.1038/nature12991

Crowley, J. L., Schoene, B., & Bowring, S. A. (2007). U-Pb dating of zircon in the Bishop Tuff at the millennial scale. *Geology*, *35*(12), 1123–1126. https://doi.org/10.1130/G24017A.1

Davaille, A., & Jaupart, C. (1993). Transient high-Rayleigh-number thermal convection with large viscosity variations. *Journal of Fluid Mechanics*, *253*(1), 141–166. https://doi.org/10.1017/S0022112093001740

Druitt, T. H., Costa, F., Deloule, E., Dungan, M., & Scaillet, B. (2012). Decadal to monthly timescales of magma transfer and reservoir growth at a caldera volcano. *Nature*, *482*(7383), 77–80. https://doi.org/10.1038/nature10706

Dufek, J., & Bachmann, O. (2010). Quantum magmatism: Magmatic compositional gaps generated by melt-crystal dynamics. *Geology*, *38*(8), 687–690. https://doi.org/10.1130/G30831.1

Edmonds, M., Aiuppa, A., Humphreys, M., Moretti, R., Giudice, G., Martin, R. S., et al. (2010). Excess volatiles supplied by mingling of mafic magma at an andesite arc volcano. *Geochemistry, Geophysics, Geosystems*, *11*, Q04005. https://doi.org/10.1029/2009GC002781

Fialko, Y., & Simons, M. (2001). Evidence for on-going inflation of the Socorro Magma Body, New Mexico, from interferometric synthetic aperture radar imaging. *Geophysical Research Letters*, *28*(18), 3549–3552. https://doi.org/10.1029/2001GL013318

Gelman, S. E., Gutiérrez, F. J., & Bachmann, O. (2013). On the longevity of large upper crustal silicic magma reservoirs. *Geology*, *41*(7), 759–762. https://doi.org/10.1130/G34241.1

Giordano, D., & Dingwell, D. (2003). Viscosity of hydrous Etna basalt: Implications for Plinian-style basaltic eruptions. *Bulletin of Volcanology*, *65*, 8–14. https://doi.org/10.1007/s00445-002-0233-2

Gregg, P. M., de Silva, S. L., Grosfils, E. B., & Parmigiani, J. P. (2012). Catastrophic caldera-forming eruptions: Thermomechanics and implications for eruption triggering and maximum caldera dimensions on Earth. *Journal of Volcanology and Geothermal Research*, *241-242*, 1–12. https://doi.org/10.1016/j.jvolgeores.2012.06.009

Hildreth, W. (1981). Gradients in silicic magma chambers: Implications for lithospheric magmatism. *Journal of Geophysical Research*, *86*(B11), 10,153–10,192. https://doi.org/10.1029/JB086iB11p10153

Hildreth, W., & Fierstein, J. (2000). Katmai volcanic cluster and the great eruption of 1912. *Geological Society of America Bulletin*, *112*(10), 1594–1620. https://doi.org/10.1130/0016-7606(2000)112<1594:KVCATG>2.0.CO;2

Hildreth, W., & Wilson, C. J. N. (2007). Compositional zoning of the Bishop Tuff. *Journal of Petrology*, *48*(5), 951–999. https://doi.org/10.1093/petrology/egm007

Holness, M. B. (2018). Melt segregation from silicic crystal mushes: A critical appraisal of possible mechanisms and their microstructural record. *Contributions to Mineralogy and Petrology*, *173*, 48. https://doi.org/10.1007/s00410-018-1465-2

Huber, C., Bachmann, O., & Manga, M. (2009). Homogenization processes in silicic magma chambers by stirring and mushification (latent heat buffering). *Earth and Planetary Science Letters*, *283*(1–4), 38–47. https://doi.org/10.1016/j.epsl.2009.03.029

Huber, C., Townsend, M., Degruyter, W., & Bachmann, O. (2019). Optimal depth of subvolcanic magma chamber growth controlled by volatiles and crust rheology. *Nature Geoscience*, *12*(9), 762–768. https://doi.org/10.1038/s41561-019-0415-6

Huppert, H. E., & Woods, A. W. (2002). The role of volatiles in magma chamber dynamics. *Nature*, *420*(6915), 493–495. https://doi.org/10.1038/nature01211

Jellinek, A. M., & DePaolo, D. J. (2003). A model for the origin of large silicic magma chambers: Precursors of caldera-forming eruptions. *Bulletin of Volcanology*, *65*(5), 363–381. https://doi.org/10.1007/s00445-003-0277-y

Lachenbruch, A. H., Sorey, M. L., Lewis, R. E., & Sass, J. H. (1976). The near-surface hydrothermal regime of Long Valley caldera. *Journal of Geophysical Research*, *81*(5), 763–768. https://doi.org/10.1029/JB081i005p00763

Lee, C.-T. A., Lee, T. C., & Wu, C.-T. (2014). Modeling the compositional evolution of recharging, evacuating, and fractionating (REFC) magma chambers: Implications for differentiation of arc magmas. *Geochimica et Cosmochimica Acta*, *143*, 8–22. https://doi.org/10.1016/j.gca.2013.08.009

Lee, C.-T. A., Morton, D. M., Farner, M. J., & Moitra, P. (2015). Field and model constraints on silicic melt segregation by compaction/hindered settling: The role of water and its effect on latent heat release. *American Mineralogist*, *100*(8–9), 1762–1777. https://doi.org/10.2138/am-2015-5121

Lesher, C. E., & Spera, F. J. (2015). Chapter 5—Thermodynamic and transport properties of silicate melts and magma. In H. Sigurdsson (Ed.), *The encyclopedia of volcanoes* (Second ed.pp. 113–141). Amsterdam: Academic Press.

Marsh, B. D. (1981). On the crystallinity, probability of occurrence, and rheology of lava and magma. *Contributions to Mineralogy and Petrology*, *78*(1), 85–98. https://doi.org/10.1007/BF00371146

McKenzie, D. (1984). The generation and compaction of partially molten rock. *Journal of Petrology*, *25*(3), 713–765. https://doi.org/10.1093/petrology/25.3.713

Michael, P. J. (1984). Chemical differentiation of the Cordillera Paine granite (southern Chile) by in situ fractional crystallization. *Contributions to Mineralogy and Petrology*, *87*(2), 179–195. https://doi.org/10.1007/BF00376223

Morgan, P., Blackwell, D. D., Spafford, R. E., & Smith, R. B. (1977). Heat flow measurements in Yellowstone Lake and the thermal structure of the Yellowstone caldera. *Journal of Geophysical Research*, *82*(26), 3719–3732. https://doi.org/10.1029/JB082i026p03719

Phipps Morgan, J., & Chen, Y. J. (1993). The genesis of oceanic crust: Magma injection, hydrothermal circulation, and crustal flow. *Journal of Geophysical Research*, *98*(B4), 6283–6297. https://doi.org/10.1029/92JB02650

Reid, M. (2013). Timescales of magma transfer and storage in the crust. In *Treatise on geochemistry* (2nd ed., pp. 181–201). Frisco, CO: Elsevier Inc.

Richardson, J., & Zaki, W. (1954). Sedimentation and fluidisation. Part 1. *Transactions. Institute of Chemical Engineers*, *32*, 35–53.

Saar, M. O., Manga, M., Cashman, K. V., & Fremouw, S. (2001). Numerical models of the onset of yield strength in crystal–melt suspensions. *Earth and Planetary Science Letters*, *187*(3-4), 367–379. https://doi.org/10.1016/S0012-821X(01)00289-8

Schmitt, A. K., Stockli, D. F., Lindsay, J. M., Robertson, R., Lovera, O. M., & Kislitsyn, R. (2010). Episodic growth and homogenization of plutonic roots in arc volcanoes from combined U–Th and (U–Th)/He zircon dating. *Earth and Planetary Science Letters*, *295*(1-2), 91–103. https://doi.org/10.1016/j.epsl.2010.03.028

Shaw, H. R. (1965). Comments on viscosity, crystal settling, and convection in granitic magmas. *American Journal of Science*, *263*(2), 120–152. https://doi.org/10.2475/ajs.263.2.120

Sisson, T. W., & Layne, G. D. (1993). H_2O in basalt and basaltic andesite glass inclusions from four subduction-related volcanoes. *Earth and Planetary Science Letters*, *117*(3-4), 619–635. https://doi.org/10.1016/0012-821X(93)90107-K

Spera, F. J., & Crisp, J. A. (1981). Eruption volume, periodicity, and caldera area: Relationships and inferences on development of compositional zonation in silicic magma chambers. *Journal of Volcanology and Geothermal Research*, *11*(2-4), 169–187. https://doi.org/10.1016/0377-0273(81)90021-4

Sutton, A. N., Blake, S., Wilson, C. J. N., & Charlier, B. L. A. (2000). Late Quaternary evolution of a hyperactive rhyolite magmatic system: Taupo volcanic centre, New Zealand. *Journal of the Geological Society*, *157*(3), 537–552. https://doi.org/10.1144/jgs.157.3.537

Tait, S., Jaupart, C., & Vergniolle, S. (1989). Pressure, gas content and eruption periodicity of a shallow, crystallising magma chamber. *Earth and Planetary Science Letters*, *92*(1), 107–123. https://doi.org/10.1016/0012-821X(89)90025-3

Troch, J., Ellis, B. S., Harris, C., Ulmer, P., & Bachmann, O. (2018). The effect of prior hydrothermal alteration on the melting behaviour during rhyolite formation in Yellowstone, and its importance in the generation of low-δ18O magmas. *Earth and Planetary Science Letters*, *481*, 338–349. https://doi.org/10.1016/j.epsl.2017.10.039

Turcotte, D. L., & Schubert, G. (2002). *Geodynamics*. Cambridge: Cambridge University Press. https://doi.org/10.1017/CBO9780511807442

Wark, D., Hildreth, W., Spear, F., Cherniak, D., & Watson, E. (2007). Pre-eruption recharge of the Bishop magma system. *Geology*, *35*(3), 235–238. https://doi.org/10.1130/G23316A.1

Wark, D. A. (1991). Oligocene ash flow volcanism, northern Sierra Madre Occidental: Role of mafic and intermediate-composition magmas in rhyolite genesis. *Journal of Geophysical Research*, *96*(B8), 13,389–13,411. https://doi.org/10.1029/90JB02666

Wilson, C. J. N. (1993). Stratigraphy, chronology, styles and dynamics of late Quaternary eruptions from Taupo volcano, New Zealand. *Philosophical Transactions of the Royal Society of London. Series A: Physical and Engineering Sciences*, *343*(1668), 205–306.

Wilson, C. J. N. (2001). The 26.5 ka Oruanui eruption, New Zealand: An introduction and overview. *Journal of Volcanology and Geothermal Research*, *112*(1-4), 133–174. https://doi.org/10.1016/S0377-0273(01)00239-6

Wilson, C. J. N., Blake, S., Charlier, B. L. A., & Sutton, A. N. (2006). The 26·5 ka Oruanui eruption, Taupo volcano, New Zealand: Development, characteristics and evacuation of a large rhyolitic magma body. *Journal of Petrology*, *47*(1), 35–69. https://doi.org/10.1093/petrology/egi066